Radiat Environ Biophys (2001) 40:1–9

ORIGINAL PAPER

Tomas Radivoyevitch · Stanislav Kozubek
Rainer K. Sachs

Biologically based risk estimation for radiation-induced CML

Inferences from *BCR* and *ABL* geometric distributions

Received: 10 August 2000 / Accepted: 20 December 2000

Abstract Chronic myeloid leukemia (CML) invites biologically based radiation risk modeling because CML is simultaneously well-understood, homogeneous and prevalent. CML is known to be caused by a translocation involving the *ABL* and *BCR* genes, almost all CML patients have the *BCR-ABL* translocation, and CML is prevalent enough that its induction is unequivocally detected among Hiroshima A-bomb survivors. In a previous paper, a linear-quadratic-exponential (LQE) dose-response model was used to estimate the lifetime excess risk of CML in the limit of low doses of γ-rays, R_γ. This estimate assumed that *BCR-ABL* translocation dose-response curves in stem cells for both neutrons and γ-rays, differ only by a common proportionality constant from dicentric aberration dose-response curves in lymphocytes. In the present paper we challenge this assumption by predicting the *BCR-ABL* dose response. The predictions are based on the biophysical theory of dual radiation action (TDRA) as it applies to recent *BCR*-to-*ABL* distance data in G_0 human lymphocytes; this data shows *BCR* and *ABL* geometric distributions that are not uniform and not independent, with close association of the two genes in some cells. The analysis speaks against the previous proportionality assumption. We compute 11 plausible LQE estimates of R_γ, 2 based on the proportionality assumption and 9 based on TDRA predictions. For each estimate of R_γ we also compute an associated estimate of the number of CML target cells, N; the biological basis of the LQE model allows us to form such estimates. Consistency between N and hematological considerations provides a plausibility check of the risk estimates. Within the group of estimates investigated, the most plausible lifetime excess risk estimates tend to lie near R_γ=0.01 Gy^{-1}, substantially higher than risk estimates based on the proportionality assumption.

T. Radivoyevitch is on temporary leave from the Department of Biometry and Epidemiology, Medical University of South Carolina, Charleston, SC 29425, USA

T. Radivoyevitch (✉) · R.K. Sachs
Department of Mathematics, University of California, Berkeley 94720, USA
e-mail: radivot@musc.edu
Tel.: +1-843-7667064, Fax: +1-843-8761126

S. Kozubek
Institute of Biophysics, Academy of Sciences, 61265 Brno, Czech Republic

Introduction

Estimating radiation-induced cancer risks probably requires a biologically based modeling step to bridge the gap between the mGy-level doses of primary interest and the typically much higher doses that are amenable to laboratory and epidemiological studies. Chromosome aberrations are associated with cancers [1] and at least for a few types of cancer, a reasonable case can be made that the aberrations are the cause of the cancer. For such cancer types there is some hope of explaining radiation carcinogenesis mechanistically and quantitatively, starting from biophysical analyses of early radiation damage, continuing through estimates of the misrejoining that makes a chromosome aberration and going systematically all the way to the epidemiological data.

Chronic myeloid leukemia (CML) [1] is ideal for biologically based radiation risk modeling because it is simultaneously well-understood, homogeneous, and prevalent. How well is it understood? There is indisputable evidence that CML is causally related to the *Bcr-Abl* chimeric protein product of a translocation between the *ABL* gene on chromosome 9 and the *BCR* gene on chromosome 22. This evidence includes increases in leukemia incidence in mice expressing *BCR-ABL* [2, 3], the association of different *BCR* exchange points with different types of leukemia [4, 5] and the finding that elevated *Bcr-Abl* tyrosine kinase activity is essential for *BCR-ABL*-mediated leukemogenesis [6]. Many experts view *BCR-ABL* as the *sine qua non* of CML [7]. Regarding its sufficiency, detection of *BCR-ABL* in healthy individuals could be the result of *BCR-ABL* arising inconsequentially in differentiated white blood cells [8, 9]. For recent reviews see [10, 11].

Almost all CML patients have the *BCR-ABL* translocation [12]. Thus, clinically defined CML can be equated to a *BCR-ABL*-mediated cancer. In this regard, CML is "homogeneous." Homogeneity is important because it allows molecular mechanistic modeling of older, clinically defined epidemiological data.

Among homogeneous cancers, such as CML and acute promyelocytic leukemia (APL), CML is one of the most prevalent. Presumably the reason is that *ABL* provides an unusually large intron target (~300 kb) for *BCR-ABL* translocations which, after RNA splicing, yield the same chimeric protein product and thus the same clinical disease. Prevalent endpoints are attractive to study because they tend to have significant numbers of induced cases in epidemiological data sets. CML is prevalent enough that its induction can be detected in A-bomb survivors [13] and in women treated with radiation [14, 15].

Preview

Our estimates of radiation-induced CML risk are based on a linear-quadratic-exponential (LQE) model [16] which contains nine parameters, five of which are dose-response shape parameters. Previously, it was found that A-bomb survivor data alone are not powerful enough to estimate three of these shape parameters [16]. These three parameters were therefore fixed to A-bomb exclusive prior means. Two of the three fixed parameters, $\beta_{ba}/\alpha_{ba\gamma}$ and $\alpha_{ban}/\alpha_{ba\gamma}$, have biological interpretations as ratios of γ-ray and neutron *BCR-ABL* dose-response parameters. Our goal here is to improve CML risk estimates by improving estimates of these two parameters. We will do this by replacing previous estimates of $\beta_{ba}/\alpha_{ba\gamma}$ and $\alpha_{ban}/\alpha_{ba\gamma}$, based on dicentric yields in human lymphocytes [17], with new estimates, predicted by an application of the theory of dual radiation action (TDRA) [18] to recent *BCR*-to-*ABL* distance data [19]. Basically, proximity between *BCR* and *ABL* has been observed in a fraction of the nuclei analyzed and this geometric association increases the chance for a *BCR-ABL* translocation relative to the chance of a "generic" dicentric or translocation, i.e. one whose two breakpoints have no special association in the cell nucleus. As we shall see, the *BCR-ABL* dose-response parameters predicted for γ-rays differ substantially from previous parameter estimates based on generic dicentrics. Fixing $\beta_{ba}/\alpha_{ba\gamma}$ and $\alpha_{ban}/\alpha_{ba\gamma}$ to their new estimates while fitting the LQE model to A-bomb survivor data, and using Bayesian methods to combine likelihood estimates with previous priors for the other parameters [16], we obtain new estimates of the lifetime excess risk of CML in the limit of low doses of γ-rays, R_γ. These risk estimates are then mapped into associated estimates of the number of CML target cells, N. Consistency between N and expectations based on hematological considerations provides a useful plausibility check of the associated risk estimates R_γ.

Materials and methods

Theory of dual radiation action (TDRA)

Our basic picture is that radiation occasionally induces contemporaneous double strand breaks (DSBs) in *ABL* and *BCR* and that the two DSBs can then react with each other to form a translocation where one of the two rearranged chromosomes carries the *BCR-ABL* sequence; an alternative scenario [20], where one break is radiation-produced and the second break is then made in an enzymatic process, will not be analyzed here. We will use the distance formulation of TDRA [18] with the "sublesions" of TDRA identified specifically as DSBs, to quantify $E(ba|D)$, the dose-response of the expected yield of such *BCR-ABL* translocations; here D is the radiation dose.

In TDRA, the geometric distance r between two DSBs at the time of their formation plays a key role. The theory provides an expression for the expected yield of translocations in the whole genome, $E(T|D)$, as an integral involving the following three functions: the energy proximity function $t_D(r)$ for radiation, defined such that $t_D(r)dr$ is the expected amount of energy deposited in a spherical shell (volume $4\pi r^2 dr$) centered at an arbitrary energy-weighted ionization point; the sensitive matrix proximity function $s(r)$, defined such that $s(r)dr$ is the expected volume of sensitive matrix (primarily DNA) within a spherical shell (volume $4\pi r^2 dr$) centered at an arbitrary point within the matrix, and the probability $g(r)$ that two DSBs misrejoin if they are created r units apart. Using these three functions, TDRA gives the expected yield of chromosomal translocations as

$$E(T|D) = \frac{1}{4} GD \int_0^\infty G \frac{t_D(r)}{\rho 4\pi r^2} \frac{s(r)}{V} g(r)dr = \frac{1}{4} GD \int_0^\infty GD(r)S(r)g(r)dr. \quad (1)$$

Here ρ is the mass density, V is the total volume of sensitive matrix per nucleus, $D(r) \equiv t_D(r)/4\pi r^2 \rho$ can be regarded as a conditional dose, $S(r) \equiv s(r)/V$ and G is the DSB yield. The integral (Eq. 1) can be interpreted as follows: consider one of GD DSBs placed at the origin. The probability that this DSB misrejoins with a DSB created r units away equals the conditional dose at r, $D(r)$, multiplied by the expected fraction of total sensitive volume that is r units away, $S(r)dr$, multiplied by G to make this the expected number of DSBs at r, multiplied by the conditional probability $g(r)$ that, given a DSB at r, this DSB misrejoins with the DSB at the origin. The model assumes complete reciprocal exchanges, with each such exchange involving two DSBs and resulting in a pair of rearranged chromosomes. Following the usual convention, we count such a pair of rearranged chromosomes as one entity (i.e. either as one translocation or as one dicentric). In accordance with recent observations, we approximate the translocation frequency as equal to the dicentric frequency [21, 22]. The factor of 1/4 in Eq. (1) accounts for two things: each DSB is counted twice in the integral and only half the misrejoining exchanges are translocations, the other half being dicentrics.

Note that by virtue of its definition, $S(r)$ is the probability density for finding sensitive matrix at r given that there is sensitive matrix at the origin. Also note that kinetics are not a part of this model: $g(r)$ maps the initial state directly into the final state without tracking the intervening evolution in time.

The energy proximity function $t_D(r)$ can be decomposed into an intra-track component $t(r)$ that depends only on radiation type and an inter-track component $\rho 4\pi r^2 D$ that depends only on dose,

$$t_D(r) = t(r) + \rho 4\pi r^2 D. \quad (2)$$

Substituting this expression into Eq. (1) yields

$$E(T|D) = \frac{1}{4} G^2 D \left(\int_0^\infty \frac{t(r)}{\rho 4\pi r^2} S(r)g(r)dr + D \int_0^\infty S(r)g(r)dr \right) \quad (3)$$

which gives a linear-quadratic dose-response $E(T|D) = \alpha_T D + \beta_T D^2$ with

$$\alpha_T = \frac{1}{4} G^2 \int_0^\infty \frac{t(r)}{\rho 4\pi r^2} S(r)g(r)dr \quad \text{and} \quad \beta_T = \frac{1}{4} G^2 \int_0^\infty S(r)g(r)dr. \quad (4)$$

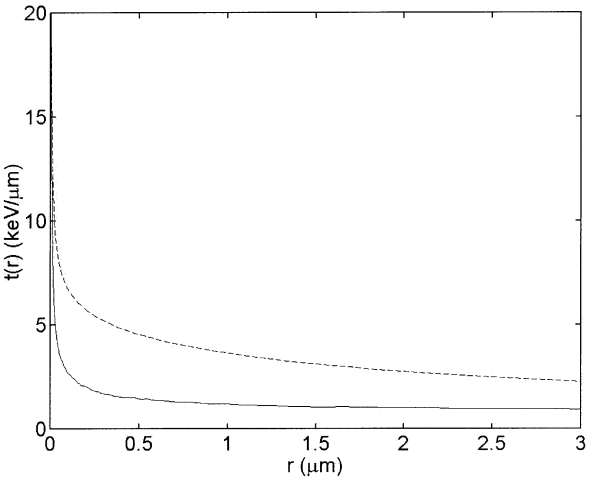

Fig. 1 Intra-track energy proximity function $t(r)$ for ^{60}Co γ-rays (*solid*) and lightly filtered x-rays (*dashed*) given in Chen et al. [25]

Estimation of $g(r)$

The interaction probability $g(r)$ is considered to be the same for generic translocations, generic dicentrics and *BCR-ABL* translocations, so we can estimate $g(r)$ from dicentric data in the literature. Appropriate assumptions for Eq. (4) are ρ=1 gm/cm^3 so that 1 Gy=6.25 keV/μm^3; G=35 DSBs per Gy per cell during G_0/G_1 [23, 24]; $E(T|D)=E(dic|D)=\alpha_d D+\beta_d D^2$, where α_d and β_d are for dicentrics ($\alpha_{d\gamma}$ for γ-rays and α_{dx} for x-rays) [21]; $g(r)=p_0 e^{-(r/r_0)}$ [18]; $S(r)$ for loci pairs distributed uniformly and independently in a nucleus of radius R:

$$S(r) = 3\frac{r^2}{R^3} - (9/4)\frac{r^3}{R^4} + (3/16)\frac{r^5}{R^6} \equiv S_0(r), \tag{5}$$

see [18], the dashed curve in Fig. 4, and Appendix A; and $t(r)$ [$t_x(r)$ for x-rays and $t_\gamma(r)$ for γ-rays] as calculated by Chen et al. [25], see Fig. 1. To estimate $g(r)$ from dicentric yield data we solve

$$\alpha_{d\gamma} = \frac{1}{4}\frac{(p_0G^2)}{6.25}\int_0^\infty t_\gamma(r)\frac{S_0(r)}{4\pi r^2}e^{-(r/r_0)}dr \tag{6a}$$

$$\alpha_{dx} = \frac{1}{4}\frac{(p_0G^2)}{6.25}\int_0^\infty t_x(r)\frac{S_0(r)}{4\pi r^2}e^{-(r/r_0)}dr \tag{6b}$$

$$\beta_d = \frac{1}{4}(p_0G^2)\int_0^\infty S_0(r)e^{-(r/r_0)}dr \tag{6c}$$

for the unknowns p_0 and r_0. Dicentric yield parameters for human lymphocytes are distributed in the literature [17, 26], very roughly speaking, as $\alpha_{d\gamma}$~U(.01, .025), α_{dx}~U(.04, .05) and β_d~U(.05, .06), where U(a,b) denotes a uniform random variable on the interval (a,b). Furthermore, based on data of Kozubek et al. [19], lymphocyte nuclei have radii R distributed normally with mean μ=3.7 μm and standard deviation σ=0.65 μm. By trial-and-error we found that Eqs. (6a–c) are solved in the literature range only when $\alpha_{d\gamma}$ lies between 0.019 Gy^{-1} and 0.024 Gy^{-1}, the boundaries being such that α_{dx}=0.04 Gy^{-1} and 0.05 Gy^{-1}, respectively. Thus, for our baseline estimate of $g(r)$ we let $\alpha_{d\gamma}$=0.022 Gy^{-1}, β_d=0.055 Gy^{-2} and R=3.7 μm, which gave r_0=0.24 μm and p_0=0.13. We then examined estimates of r_0 and p_0 at the boundaries of α_{dx} when β_d equaled 0.05 Gy^{-2} and 0.06 Gy^{-2}, and when R equaled 3.7 μm or 3 μm. We found that our estimates were insensitive to β_d and that only p_0 was sensitive to R. Plausible point and interval estimates were thus found to be r_0=0.24 μm (0.23, 0.26) and p_0=0.13 (0.14, 0.06) – asymmetric intervals result because R=3 μm is supported [26] while R=4.5 μm is not.

In Eq. (6) and throughout the rest of this paper, G and p_0 never appear separately, only in the combination p_0G^2, and it is only this combination which affects the final estimates; for example, if we had chosen G two times larger, as 70 DSBs per Gy, the estimate for p_0 would be decreased by a factor of 4 with further calculations and results essentially unchanged.

Adaptation of TDRA for specific loci

The TDRA distance model can be adapted for *BCR-ABL* dose-response predictions as follows. Assuming a *BCR* target size T_{BCR} of 5.8 kbp [5], an *ABL* target size T_{ABL} of 300 kbp [5], and a human genome size Γ of 3,200 Mb [27], the expected number of active DSBs within the *BCR* target is $(T_{BCR}/\Gamma)GD$ and the expected number of DSBs within the *ABL* target is $(T_{ABL}/\Gamma)GD$. Let $S_{ba}(r)$ be the normalized probability density of *BCR*-to-*ABL* distances r, i.e. let $S_{ba}(r)dr$ be the fraction of the *ABL* target material expected at r given that there is *BCR* target material at the origin. Letting each of the expected $(T_{BCR}/\Gamma)GD$ DSBs in *BCR* serve as the origin, the expected number of *ABL* DSBs a distance r away becomes $(T_{ABL}/\Gamma)GD(r)S_{ba}(r)dr$. Thus

$$E(ba|D) = \frac{T_{BCR}T_{ABL}G^2D}{2\Gamma^2}\int_0^\infty \frac{t_D(r)}{\rho 4\pi r^2}S_{ba}(r)g(r)dr. \tag{7a}$$

Here a factor 1/2 applies, instead of 1/4 as in Eq. (1), because here the integral does not count each DSB twice. Note that Eq. (7a) is completely symmetric with respect to *BCR* and *ABL*, i.e. that DSBs within *ABL* could have also served as the origin. Defining α_{BA} and β_{BA} such that

$$\begin{aligned} E(ba|D) &= \alpha_{ba}D + \beta_{ba}D^2 = \frac{2T_{BCR}T_{ABL}}{\Gamma^2}(\alpha_{BA}D + \beta_{BA}D^2) \\ &= 3.4x10^{-10}(\alpha_{BA}D + \beta_{BA}D^2), \end{aligned} \tag{7b}$$

a key assumption in our previous work [16, 28] was that the *BCR-ABL* translocation process was a typical exchange process as represented by dicentrics in the whole genome, i.e.

$$\alpha_{BA}D + \beta_{BA}D^2 = \alpha_dD + \beta_dD^2. \tag{8}$$

Granting equality of dicentrics and translocations, Eq. (8) is equivalent to assuming $S_{ba}(r)=S_d(r)$ in TDRA because, with $g(r)$ and $t(r)$ fixed, the dose-response depends only on $S(r)$; here $S_d(r)$ is the inter-loci distance probability density for generic loci-pairs in the whole genome.

Ideally, interphase fluorescence in situ hybridization (FISH) data would provide independent estimates of $S_{ba}(r)$ and $S_d(r)$. $S_d(r)$ together with data for dicentrics in the whole genome could then provide an estimate of $g(r)$, and $g(r)$ and $S_{ba}(r)$ could then predict the *BCR-ABL* dose-response. Without $S_d(r)$ data, an assumption must be made. Assuming $S_d(r)=S_{ba}(r)$ yields Eq. (8) and our previous results [16, 28]. Assuming $S_d(r)=S_0(r)$ gives $g(r)$ above and the predictions described below. Some support for the assumption $S_d(r)=S_0(r)$ comes from the following perspective. Viewing $S_d(r)$ as the target-size weighted-average of $S_{ij}(r)$ over all possible loci pairs ij, i.e.

$$S_d(r) = \sum_i\sum_j \frac{T_iT_j}{\Gamma^2}S_{ij}(r),$$

some loci pairs in this sum will tend to be close, such as those between chromosomes 9 and 22, and some loci pairs will tend to be far apart, such as those between chromosomes 8 and 9 [19]. It seems plausible that such extremes will average out and thus that $S_d(r)\approx S_0(r)$.

BCR-to-*ABL* distance data

The data sets used have been described [19, 29]. The G_0 human lymphocyte data set of Kozubek et al. [19] contains two-dimensional (2D) projection measurements of the *BCR* and *ABL* positions. Measurements made in 5,735 cells provide 22,940 *BCR*-to-

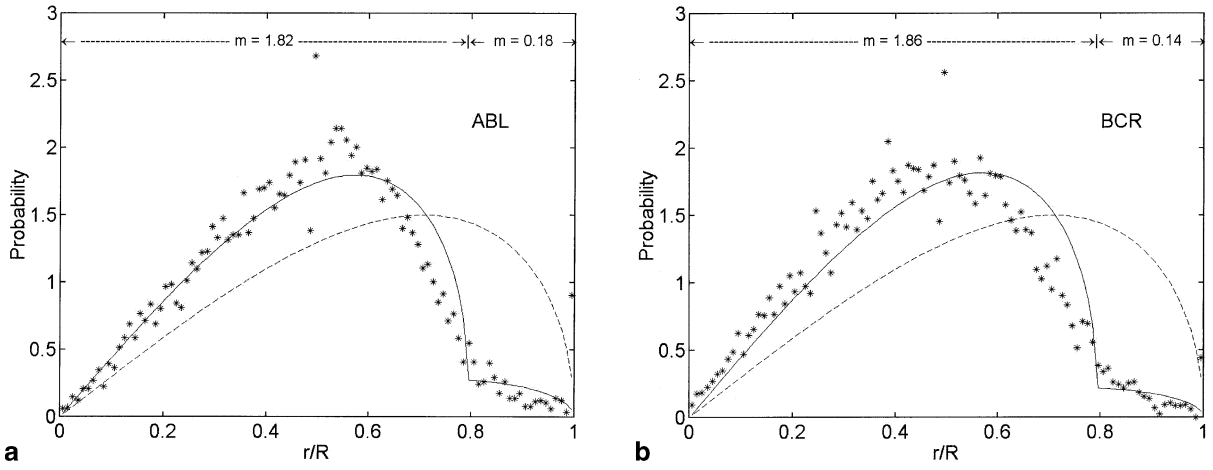

Fig. 2a, b The 2D loci-to-center data of Kozubek et al. [19] (G_0 human lymphocytes) fit to the two-shell RS model. The piece-wise constant relative mass densities are shown above the curves (see Table 1). The dashed curves are for a uniform density, i.e. a one-shell model with a relative mass density of one

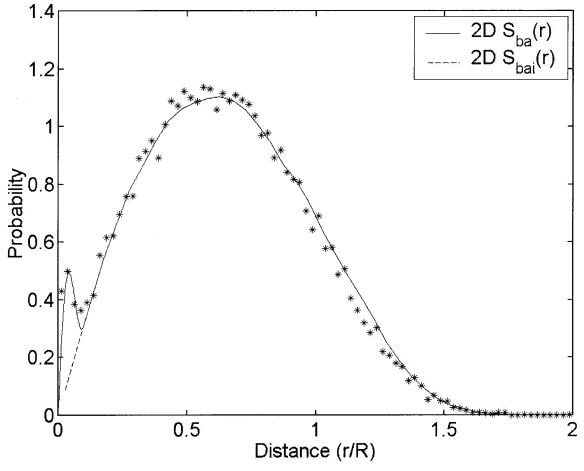

Fig. 3 2D *BCR*-to-*ABL* data. The solid curve is the 2D equivalent of $S_{ba}(r)$ predicted for correlated loci (Eq. 13), i.e. 2% of the loci pairs tethered within a uniform density sphere of radius 0.05*R*, *R* being the radius of the nucleus. The dashed curve is the 2D equivalent of $S_{bai}(r)$ predicted by the two shell RS model with independent loci; it coincides visually with the solid curve except at small *r*

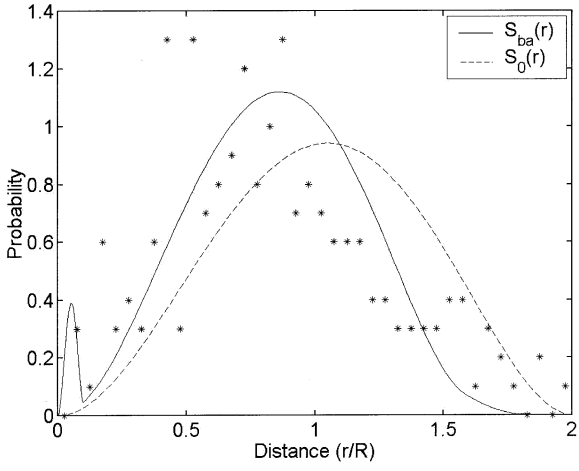

Fig. 4 Comparison between $S_{ba}(r)$ and the 3D *BCR*-to-*ABL* data of Neves et al. [29] (human CD34$^+$ stem cells in G_1). Shown dashed is $S_0(r)$

ABL distances (Fig. 2) and for each gene, 11,470 distances to the center of the nucleus (Fig. 3). The cells were from a single individual – results from other individuals were similar although the number of cells analyzed was much lower. The G_0 lymphocyte data [19] used here are representative of stimulated lymphocytes, bone-marrow cells, HL-60 cells and U-937 cells [30]. In all of these cell types *ABL* and *BCR* are distributed non-uniformly, and in some of these cell types correlations are observed.

The 3D confocal FISH data of Neves et al. [29] consist of 200 *BCR*-to-*ABL* distance measurements (Fig. 4) in 50 G_1-phase CD34$^+$ human hematopoietic stem cells. Relative to the Kozubek data, this data set is attractive because CD34$^+$ stem cells are more relevant to CML than lymphocytes and because 3D measurements are more informative than 2D measurements. However, with only 200 distance measurements, the number in the small *r* bins is not large enough to resolve $S_{ba}(r)$ where it matters the most (compare Figs. 3 and 4). Use of this CD34$^+$ data set will therefore be limited to comparisons.

The rotational symmetry model

Suppose we have a spherical nucleus of radius *R* and suppose *r* is the distance from its center. In the rotational symmetry (RS) model [31, 32] the sensitive matrix has an expected relative mass density $m(r)$ that depends only on *r*, i.e. it is spherically symmetric. The relative mass density $m(r)$ is defined as the mass density relative to the constant mass density ρ_c that would have resulted had the same amount of target material been uniformly distributed throughout the nucleus, i.e. $m(r)$ is a dimensionless quantity that satisfies

$$M = \rho_c \frac{4}{3}\pi R^3 = \rho_c \int_0^R m(r) 4\pi r^2 dr \quad \text{and thus} \quad \int_0^R m(r) 4\pi r^2 dr = \frac{4}{3}\pi R^3. \tag{9}$$

If the target material is indeed uniformly distributed, then $m(r)=1$. We will consider piece-wise constant $m(r)$ where the breakpoints in the function are defined such that $m(r)$ is constant within *n* concentric shells of equal volume – equal volumes help distribute distance measurements evenly across bins. With piecewise constant $m(r)$, Eq. (9) implies $m(r) \le n$.

Appendix A provides a means of mapping 3D $m(r)$ functions into 3D $S(r)$ functions. Appendix B describes how 3D $m(r)$ func-

tions can be mapped into (and thus estimated from) 2D $m(r)$ data. Finally, Monte Carlo methods provide a means of mapping 3D $m(r)$ functions into 2D $S(r)$ functions. In each of these mappings the RS model is implicitly assumed in $m(r)$. Use of 2D data requires that some such assumption be made. The advantage of 3D confocal microscopy is that it directly measures the TDRA critical entity $S(r)$, i.e. it eliminates the need for the RS assumption and the 2D-3D mappings.

The LQE model

The LQE dose-response model of CML risk is described in a previous paper [16]. Briefly, it is

$$m_i = \left[e^{c_1+ka_i} + \left(D_{\gamma i} + \frac{\beta_{ba}}{\alpha_{ba\gamma}} D_{\gamma i}^2 + \frac{\alpha_{ban}}{\alpha_{ba\gamma}} D_{ni} \right) t_i^2 e^{c_2-k_t t_i} \right] \cdot P_i e^{-\left(\alpha_{k\gamma} D_{\gamma i} + \beta_k D_{\gamma i}^2 + \alpha_{kn} D_{ni}\right)} \quad (10)$$

where m_i, a_i, P_i, t_i, $D_{\gamma i}$ and D_{ni} denote the expected number of CML cases, the average age, the person-years, the average number of years since exposure, and the average gamma and neutron marrow doses, respectively, for the ith grouped epidemiological data cell. Here $\alpha_{ba\gamma}D_{\gamma i}+\alpha_{ban}D_{ni}+\beta_{ba}(D_{\gamma i}+D_{ni})^2 \approx \alpha_{ba\gamma}D_{\gamma i}+\beta_{ba}D_{\gamma i}^2+\alpha_{ban}D_{ni}$ is the probability of forming *BCR-ABL* in a target cell (the approximation follows since $D_{\gamma i} >> D_{ni}$ among A-bomb survivors [33]), $e^{-(\alpha_{k\gamma}D_{\gamma i}+\beta_k D_{\gamma i}^2+\alpha_{kn}D_{ni})}$ is the probability that the target cell is not killed, $e^{c_1+ka_i}$ is the background incidence as a function of age, and $t_i^2 e^{c_2-k_t t_i}$ represents the *BCR-ABL*-to-CML waiting time probability density $w(t) = \frac{k_t^3 t^2}{2} e^{-k_t t}$ multiplied by $N\alpha_{ba\gamma}$ where N is the number of target cells, i.e. $e^{c_2} = N\alpha_{ba\gamma}\frac{k_t^3}{2} = N\frac{2T_{BCR}T_{ABL}}{\Gamma^2}\alpha_{BA\gamma}\frac{k_t^3}{2}$.

Using A-bomb exclusive data, estimates can be obtained for each of the nine parameters of the LQE model. These "prior" parameter estimates can then be combined with A-bomb survivor data in a Bayesian approach to CML risk estimation. For details and explanations, see [16]. In this paper, we will replace previous assumptions that $\beta_{ba}/\alpha_{ba\gamma}=\beta_d/\alpha_{d\gamma}$ and $\alpha_{ban}/\alpha_{ba\gamma}=\alpha_{dn}/\alpha_{d\gamma}$ with new assumptions based on TDRA and *BCR*-to-*ABL* distance data, i.e. Eqs. (7). Our goal then is to see how these changes modify both the lifetime excess risk of CML in the limit of low doses of γ-rays,

$$R_\gamma = \int_0^\infty t^2 e^{c_2-k_t t} dt = \frac{2e^{c_2}}{k_t^3} = N\alpha_{ba\gamma}, \quad (11)$$

and its associated estimate of the number of CML target cells

$$N = R_\gamma / \alpha_{ba\gamma} = \frac{R_\gamma \Gamma^2}{2T_{BCR}T_{ABL}\alpha_{BA\gamma}}. \quad (12)$$

Comment: Whereas the dose-response structure of the LQE model is biologically based, the background and waiting time structures are not. These structures derive instead from empirical fits to A-bomb exclusive epidemiological data. The LQE model could thus be more accurately described as semi-biologically based, rather than biologically based.

Results

Estimation of $S_{ba}(r)$

We assume a piece-wise constant RS model with two equal volume shells, i.e. a model where the expected relative mass density $m_b(r)$ of *BCR* target material, $m_a(r)$ for *ABL*, is constant within a sphere and its surrounding spherical shell. Fitting this model to recent 2D data [19] produces the results shown in Fig. 2 and Table 1. Fitting it to recent 3D data [29] for comparison, assuming $m_a(r)=m_b(r)$ and no correlations, yields $m(r)$ as also given in Table 1. The data clearly suggest that more often than not, *BCR* and *ABL* lie within the inner half of the nucleus.

Assuming independence of the loci positions, Monte Carlo methods were used to map the 3D reconstructions $m_b(r)$ and $m_a(r)$ into an expected 2D *BCR*-to-*ABL* distance probability density as shown in Fig. 3 (for small r this is the dashed curve). This curve, derived from 2D locus-to-center data, is compared, not fit, to the *BCR*-to-*ABL* 2D distance data of the same experiment [19]. Note that the theoretical values are well below the observed data for small r. This discrepancy suggests that the loci positions are not actually independent. Since $S_{ba}(r)$ for small r is critical to TDRA predictions, modeling such loci correlation is essential. Our model of it is as follows. For some small percentage of time, or equivalently for our purposes, at any one time point, for some small percentage p of loci pairs, we hypothesize that there exists a "bond" between chromosomes 9 and 22 that tethers *BCR* and *ABL* to within a small sphere of radius κR, $\kappa<1$. The solid curve in Fig. 3 is then the 2D equivalent of

$$S_{ba}(r) = p\frac{1}{\kappa}S_0(r/\kappa) + (1-p)S_{bai}(r) \quad (13)$$

where p=0.02 [0.016, 0.24] and κ=0.05 [0.04, 0.06] were determined by visual trial-and-error; here $S_{bai}(r)$ is for independent loci. In Fig. 4 we compare this model of $S_{ba}(r)$ to the 3D *BCR*-to-*ABL* distance data of Neves et al. [29].

The *BCR-ABL* dose-response

Next we applied TDRA to $S_{ba}(r)$ in Eq. (13). Using $g(r) = p_0 e^{-(r/r_0)}$ with the parameter estimates r_0=0.24 μm [0.23, 0.26] and p_0=0.13 [0.14, 0.06] discussed above, and using $t(r)=t_\gamma(r)$ for γ-rays as given by Chen et al. [25], our main result is the TDRA prediction that $\alpha_{BA\gamma}$=3.64 [2.5, 4.3] Gy^{-1} and β_{BA}=0.45 [0.29, 0.49]

Table 1 The two-shell RS model fit to the data in Figs. 2 and 4

Parameter	Ref. [19] and Fig. 2		Ref. [29] and Fig. 4
	$m_a(r)$	$m_b(r)$	$m_a(r)=m_b(r)$
0<r<0.79R	1.82 (1.78, 0.86)[a]	1.86 (1.82, 1.90)	1.52 (1.3, 1.8)
0.79R<r<R	0.18 (0.16, 0.20)	0.14 (0.13, 0.16)	0.48 (0.3, 0.7)

[a] In parenthesis are the 95% CI

Table 2 Dependence of R_γ and N on the choice of fixed LQE parameters $\beta_{ba\gamma}/\alpha_{ba\gamma}$ and $\alpha_{ban}/\alpha_{ba\gamma}$

Row#	$\beta_{BA\gamma}/\alpha_{BA\gamma}$[a]	$\alpha_{BAn}/\alpha_{BA\gamma}$[a]	R_γ(Gy^{-1})	N	Notes
1	.055/.0107	.8/.0107	.0022 (.0012, .0039)[b]	6.1×10^8 (3.3×10^8, 1.1×10^9)	$\alpha_{d\gamma}$=0.0107 Gy^{-1}
2	.055/.022	.8/.022	.0039 (.0020, .0073)	5.2×10^8 (2.7×10^8, 9.8×10^8)	$\alpha_{d\gamma}$=0.022 Gy^{-1}
3	.45/3.64	.8/.022[c]	.0094 (.0051, .0176)	7.6×10^6 (4.1×10^6, 1.4×10^7)	Baseline $g(r)$
4	.45/3.64	3∗.8/.022[d]	.0056 (.0029, .0106)	4.5×10^6 (2.3×10^6, 8.6×10^6)	$\alpha_{BAn}/\alpha_{dn}=3*\alpha_{BA\gamma}/\alpha_{d\gamma}$
5	.45/3.64	(1/3)∗.8/.022[d]	.0116 (.0065, .0216)	9.4×10^6 (5.3×10^6, 1.7×10^7)	$\alpha_{BAn}/\alpha_{dn}=(1/3)*\alpha_{BA\gamma}/\alpha_{d\gamma}$
6	.45/3.64	10∗.8/.022[d]	.0027 (.0014, .0052)	2.2×10^6 (4.2×10^6, 1.1×10^6)	$\alpha_{BAn}/\alpha_{dn}=10*\alpha_{BA\gamma}/\alpha_{d\gamma}$
7	.45/3.64	(1/10)∗.8/.022[d]	.0128 (.0072, .0237)	1.0×10^7 (5.8×10^6, 1.9×10^7)	$\alpha_{BAn}/\alpha_{dn}=(1/10)*\alpha_{BA\gamma}/\alpha_{d\gamma}$
8	.285/2.7	.8/.019[c]	.0091 (.0051, .0169)	1.0×10^7 (5.6×10^6, 1.8×10^7)	$g(r)$ with R=3 μm
9	.49/4.0	.8/.024[c]	.0102 (.0057, .0188)	7.5×10^6 (4.2×10^6, 1.4×10^7)	$g(r)$ with α_{dx}=0.05 Gy^{-1}
10	.29/4.29	.8/.022[c]	.0100 (.0056, .0183)	6.8×10^6 (3.8×10^6, 1.3×10^7)	$S_{ba}(r)$ with (p,κ)=(0.016, 0.04)
11	.33/2.54	.8/.022[c]	.0098 (.0054, .0184)	1.1×10^7 (6.3×10^6, 2.1×10^7)	$S_{ba}(r)$ with (p,κ)=(0.024, 0.06)

[a] Note that $\beta_{BA\gamma}/\alpha_{BA\gamma}=\beta_{ba\gamma}/\alpha_{ba\gamma}$ and $\alpha_{BAn}/\alpha_{BA\gamma}=\alpha_{ban}/\alpha_{ba\gamma}$, i.e. the numbers here enter directly into the LQE model

[b] In parentheses are the 95% CI

[c] These assume that $x=(\alpha_{BAn}/\alpha_{dn})/(\alpha_{BA\gamma}/\alpha_{d\gamma})=1$, i.e. that the neutron α increases as much as the γ-ray α

[d] These assume x=3, 1/3, 10 and 1/10

Gy^{-2}. Thus, in contrast to our previously held assumption shown in Eq. (8), $\alpha_{BA\gamma}$ is much greater than $\alpha_{d\gamma}\approx0.022$ Gy^{-1}, and β_{BA} is greater than $\beta_d\approx0.055$ Gy^{-2}; that is, the *BCR-ABL* dose-response parameters predicted by TDRA, taking deviations from randomness and independence in the geometric locations of the two loci into account, differ from the literature values [17, 26] for generic dicentrics. The new *BCR-ABL* dose-response has an amplitude parameter α that is 160-fold higher than before, and a dose-response shape parameter α/β (the linear-to-quadratic transition dose) that is 20-fold higher, i.e. 8 Gy compared to 0.4 Gy. The intuitive reason α and β both increase is that two nearby loci are more likely to interact than are two distant loci; the intuitive reason α increases even more than β is that two nearby loci are more likely to get DSBs from the same photon than are two distant loci.

Risk and target cell estimates

For reasons described elsewhere [16], only the Hiroshima male portion of the A-bomb survivor data set is used in our analysis [13]. We assume that $t_\gamma(r)$ for ^{60}Co γ-rays [25] is approximately valid for Hiroshima γ-rays and thus that the *BCR-ABL* dose-response predictions of the previous subsection are applicable. For neutrons, we do not have $t_n(r)$ and therefore cannot predict α_{ban}. Instead, we will consider two hypothetical cases: α_{ban} increasing as much as $\alpha_{ba\gamma}$ (rows 3, 8–11 of Table 2), and α_{ban} increasing x-fold more (or less) than $\alpha_{ba\gamma}$ (rows 4–7 in Table 2). Table 2 shows estimates of R_γ and N produced using random samples from bivariate normal LQE posterior estimates of c_2 and k_t, see Eqs. (11) and (12). Various possibilities are considered. Rows 1–2 assume $\beta_{ba}/\alpha_{ba\gamma}=\beta_d/\alpha_{d\gamma}$ and $\alpha_{ban}/\alpha_{ba\gamma}=\alpha_{dn}/\alpha_{d\gamma}$, rows 3–11 assume TDRA predictions for $\beta_{ba}/\alpha_{ba\gamma}$ and $\alpha_{ban}/\alpha_{ba\gamma}$ via Eq. (7). More specifically, in row 1 we have $\alpha_{BA\gamma}=\alpha_{d\gamma}=0.0107$ Gy^{-1}, as in [16]; in row 2, for comparisons with rows 3–11, we have $\alpha_{BA\gamma}=\alpha_{d\gamma}=0.022$ Gy^{-1}; in rows 3–7 we have $g(r)$ with baseline parameter values while $x\equiv(\alpha_{BAn}/\alpha_{dn})/(\alpha_{BA\gamma}/\alpha_{d\gamma})$ takes various values: in rows 8 and 9 other plausible $g(r)$ are examined and finally, in rows 10 and 11 other $S_{ba}(r)$ are tested. The results of these cases are summarized in Table 2 and discussed fully below.

Discussion

In previous work we found that A-bomb survivor data does not have the power to estimate more than one or two of the five LQE dose-response shape parameters [16]. Three of the LQE dose-response shape parameters ($\beta_{ba}/\alpha_{ba\gamma}$, $\alpha_{ban}/\alpha_{ba\gamma}$ and α_{kn}) were therefore fixed to prior means. In general, fixing parameters converts statistical uncertainty into model assumption uncertainty. This notion is supported in Table 2 by the observation that row variation exceeds estimate uncertainty. Thus, LQE modeling uncertainty dominates LQE statistical uncertainty.

The LQE model under the previous assumption of Eq. (8) yields $R_\gamma=0.0022$ Gy^{-1} [16] or $R_\gamma=0.0039$ Gy^{-1}, depending on the assumed value of the dicentric yield parameter $\alpha_{d\gamma}$ (see rows 1 and 2 of Table 2). Meanwhile, using *BCR*-to-*ABL* distance data and TDRA, the LQE model yields the range of risk estimates given in rows 3–11 (Table 2). Although the two groups have slightly overlapping estimates of R_γ, they can be separated cleanly by their associated estimates of N.

There is general agreement among hematologists that there are about 10^{12} nucleated marrow cells per adult [34], that there is approximately one LTC-IC (long-term culture-initiating cell) per 10^5 nucleated marrow cells [11, 35] and that CML target cells are probably very primitive hematopoietic stem cells [11], such as LTC-ICs. Thus, estimates of N on the order of 10^7, such as those shown in rows 3, 5, and 7–11 (Table 2), are quite consistent with hematological considerations. This is in sharp contrast with estimates on the order of more than 10^8 in rows 1 and 2, or in [28, 36], and estimates closer to 10^6 in rows 4 and 6. This suggests that risk estimates

in rows 3, 5, and 7–11 may be better than those of rows 1, 2, 4 and 6. Interestingly, the "better" risk estimates tend to cluster near R_γ=0.010 Gy^{-1}.

Since $t_n(r)$ for the Hiroshima neutron exposure is not available, we resorted (rows 3–7 of Table 2) to examining five possible neutron scenarios. The scenarios are $x\equiv(\alpha_{BAn}/\alpha_{dn})/(\alpha_{BA\gamma}/\alpha_{d\gamma})$=1, 3, 1/3, 10 and 1/10, where x is the increase in the neutron α relative to the increase in the γ-ray α. We found that as x decreases below 1/10, R_γ and N reach limiting values because the CML risk is then completely attributed to γ-rays. In this limit $N\sim1\times10^7$ is completely consistent with stem cell expectations (see row 7). In the opposite limit, as x becomes large, R_γ approaches zero because CML risk is then attributed completely to neutrons. In this limit $N\sim10^6$ target cells is below expectations. Taken together, these results suggest that x<1 is more likely than x>1. As additional support that x<1, we note that with $S_{ba}(r)$ shifting to smaller r [relative to $S_0(r)$], the correlation integral of Eq. (7a) should have a greater relative increase for $t_\gamma(r)$ in Fig. 1, than for a high, but perhaps relatively flat, $t_n(r)$.

The spatial correlation observed between the *BCR* and *ABL* positions was modeled here as a "bond" between chromosomes 9 and 22. We do not know the nature of this bond. Perhaps tetraplex hybridization occurs between Alu sequences, perhaps the nuclear matrix holds *BCR* and *ABL* in close proximity through matrix attachment regions. Regardless of how, our model predicts that unbonded states are 50 times more common than bonded states, and it predicts that the average tethering distance is about 0.05 times the nuclear radius. Additional 3D confocal experiments are needed to substantiate this claim; the distribution peak at small values of r/R was repeatedly observed in G_0-lymphocytes but the possibility of unknown systematic errors cannot be ruled out.

Our results show that, despite many uncertainties in models and parameters, a systematic, quantitative, biologically based model of radiation-induced CML may not be wholly out of reach. Some cancers other than CML might also be amenable to such analysis. One possibility is *H4-RET*-mediated papillary thyroid cancer (PTC). Recent evidence suggests that *H4* and *RET* are "tethered" even more dramatically than *BCR* and *ABL* [37]. Furthermore, PTC is certainly prevalent enough that its dose-response can be detected epidemiologically [38].

Acknowledgement We thank Drs. D. J. Brenner and J. Chen for sharing their results, Drs. L. Parreira and C. Ramos for use of their CD34$^+$ data (Fig. 4), and M. Vazquez for discussions. This publication was supported in part by funds from NIH grants GM57245-03 and CA86823, DOE grant DE-FG03-00ER62909, and the Ministries of the Czech Republic (NM-15-3, VS-97031 and 202/96/0874). This report makes use of data obtained from the Radiation Effects Research Foundation (RERF) in Hiroshima, Japan. RERF is a private foundation funded equally by the Japanese Ministry of Health and Welfare and the US Department of Energy through the US National Academy of Sciences. The conclusions in this report are those of the authors and do not necessarily reflect the scientific judgment of RERF or its funding agencies.

Appendix A

This section describes a means of mapping rotationally symmetric (RS) expected relative mass densities $m(r)$ into pair-wise distance probability density functions $S(r)$. Suppose we have a sphere of radius R and suppose that $m(r)$ satisfies Eq. (9). The probability density that a point is a distance r from the center of the sphere is then

$$f(r) = m(r)\frac{3r^2}{R^3}. \tag{A1}$$

To express $S(r)$ in terms of $f(r)$, we condition it on the two points being distances r_1 and r_2 from the center, i.e.

$$S(r) = \iint p(r|r_1,r_2) f(r_1) f(r_2) dr_1 dr_2. \tag{A2}$$

Our goal then is to find $p(r|\ r_1,r_2)$. To this end, let $\mathbf{r}_2$ be a vector extending from the origin of 3D space to the north pole of a very thin concentric shell of radius r_2 and let $\mathbf{r}_1$ be a vector to an arbitrary point on a very thin shell of radius r_1, $0<r_1$, $r_2<R$. Let θ be the angle between these two vectors. The probability of θ is then $1/2\ \sin(\theta)d\theta$ and this must equal $p(r|\ r_1,r_2)dr$. Using the law of cosines

$$r^2 = r_1^2 + r_2^2 + 2r_1r_2\cos(\theta) \Rightarrow 2rdr = 2r_1r_2\sin(\theta)d\theta$$

which then implies that $p(r|\ r_1,r_2)=r/(2r_1r_2)$. Substituting this and (A1) into (A2) yields

$$S(r) = \frac{9r}{2R^6}\iint r_1r_2m(r_1)m(r_2)dr_1dr_2 \tag{A3}$$

where complicated integration limits (not shown) are simplified by the 45° rotation

$$x_1 = \frac{1}{\sqrt{2}}(r_1 - r_2), \quad x_2 = \frac{1}{\sqrt{2}}(r_1 - r_2),$$

the inverse of which is

$$r_1 = \frac{1}{\sqrt{2}}(x_1 + x_2), \quad r_2 = \frac{1}{\sqrt{2}}(-x_1 + x_2).$$

We then have

$$r_1r_2 = \frac{1}{2}(x_2^2 - x_1^2)$$

and

$$S(r) = \frac{9r}{4R^6}\int_{-r/\sqrt{2}}^{r/\sqrt{2}}\int_{r/\sqrt{2}}^{x_1+\sqrt{2}}(x_2^2 - x_1^2)m(x_1,x_2)m(x_1,x_2)dx_2dx_1 \tag{A4}$$

This integral can be solved symbolically for $m(r)=(3+k)r^k/3R^k$ and $k=\{-1,0,1,2,\ldots\}$. The simplest examples include $k=-1$, which gives

$$S_{-1}(r) = \frac{4r^2}{R_3} - \frac{3r^3}{R_4} \quad (r<R)$$

and

$$S_{-1}(r) = \frac{4r}{R^2} - \frac{4r^2}{R^3} + \frac{r^3}{R^4} \quad (R<r<2R),$$

k=0, which reproduces the familiar $S_0(r)$ given in Eq. (5), and k=1, which gives

$$S_1(r) = \frac{16r^2}{5R^3} - \frac{4r^3}{R^4} + \frac{16r^4}{9R^5} - \frac{2r^7}{15R^8} \qquad (r < R)$$

and

$$S_1(r) = \frac{16r}{9R^2} - \frac{16r^2}{5R^3} + \frac{4r^3}{R^4} - \frac{16r^4}{9R^5} + \frac{2r^7}{45R^8} \quad (R < r < 2R).$$

Visual examination of solutions for higher k suggest that for k even, a single expression is valid for both regions of r, and for k odd, two expressions are needed. The solutions also suggest that for k odd, the solution in the second region relates to the first by a change in signs, division of the highest power term by three, and the addition of a linear term. Note for k=0 and small r that $S_0(r)$ equals $f(r)$, i.e. in this case the center of the sphere is as good a point partner as any other.

The integral of Eq. (A4) can be solved numerically for arbitrary $m(r)$. When we fit the Neves data to the two-shell model we solved this integral within each function evaluation of a log-likelihood optimization. The integral of Eq. (A4) can be readily extended to situations where $m_a(r) \neq m_b(r)$. Programs for this in Matlab are available upon request from radivot@musc.edu.

Appendix B

In this section we describe a means of mapping $m(r)$ from 3D to 2D. This mapping was used in the curve fits of Fig. 2.

The set up is as follows. In 3D, consider a thin concentric shell of radius r_s, a point on this shell that makes an angle θ with the z-axis, and the 2D projection radius of this point r_c. By mass balance we then have

$$m_s(r_s) 2\pi r_s \sin(\theta) r_s d\theta dr_s = m_c(r_c) 2\pi r_c dr_c$$

where $m_s(r_s)$ and $m_c(r_c)$ are the 3D and 2D relative mass densities, respectively, s stands for spherical and c stands for circular. Since $r_s \sin(\theta) = r_c$, we then have

$$m_s(r_s) r_s d\theta dr_s = m_c(r_c) dr_c.$$

Holding r_s fixed and varying θ, $r_s \cos(\theta) d\theta = dr_c$. Thus, the contribution that the thin 3D spherical shell makes to the 2D mass density at r_c is

$$\frac{m_s(r_s)}{\cos(\theta)} dr_s = m_c(r_c).$$

Integrating these contributions over all possibilities, i.e. from r_s=r_c to r_s=R, noting that there are two contributions above and below the x-y plane, and noting that

$$\cos(\theta) = \frac{\sqrt{r_s^2 - r_c^2}}{r_s}, \quad \text{we have} \quad m_c(r_c) = 2\int_{r_c}^{R} \frac{m_s(r_s) r_s}{\sqrt{r_s^2 - r_c^2}} dr_s. \tag{B1}$$

For piece-wise constant $m_s(r_s)$ the integrand in Eq. (B1) can be trivially integrated over each region. The net result is that $m_c(r_c)$ becomes a weighted sum of basis functions where the weights are the constant mass densities for a region and the basis functions are determined by the breakpoints in the radius r_s. For example, the basis function generated by the shell between b_i and b_{i+1} is

$$\frac{3r_c}{R^3}\sqrt{b_i^2 - r_c^2} \quad \text{for} \quad b_i < r_c < b_{i+1}$$

and

$$\frac{3r_c}{R^3}\left(\sqrt{b_{i+1}^2 - r_c^2} - \sqrt{b_i^2 - r_c^2}\right) \quad \text{for} \quad r_c < b_i.$$

Let this basis function be the ith column of a matrix **H**. The solution $\mathbf{m}_c(r_c)$ then becomes the product of **H** and a column vector m of constant relative mass densities $\mathbf{m}_i$. Thus, during our log-likelihood optimization that created the curve fits of Fig. 2, the matrix **H** was created once globally and each function evaluation merely formed **Hm** for each new **m**. Note that the constraint in Eq. (9) still applies and that it is non-linear in the parameters c_i where $\mathbf{m}_i = \exp(c_i)$.

References

1. Mitelman F (2000) Recurrent chromosome aberrations in cancer. Mutat Res 462:247–253
2. Daley GQ, Van Etten RA, Baltimore D (1990) Induction of chronic myelogenous leukemia in mice by the P210 bcr/abl gene of the Philadelphia chromosome. Science 247:824–830
3. Heisterkamp N, Jenster G, ten Hoeve J, Zovich D, Pattengale PK, Groffen J (1990) Acute leukaemia in bcr/abl transgenic mice. Nature 344:251–253
4. Voncken JW, Kaartinen V, Pattengale PK, Germeraad WT, Groffen J, Heisterkamp N (1995) BCR/ABL P210 and P190 cause distinct leukemia in transgenic mice. Blood 86:4603–4611
5. Melo JV (1996) The diversity of BCR-ABL fusion proteins and their relationship to leukemia phenotype. Blood 88:2375–2384
6. Zhang X, Ren R (1998) Bcr-Abl efficiently induces a myeloproliferative disease and production of excess interleukin-3 and granulocyte-macrophage colony-stimulating factor in mice:a novel model for chronic myelogenous leukemia. Blood 92:3829–3840
7. Cotran RS, Kumar V, Robbins SL (1994) Pathological basis of disease. Saunders, Philadelphia
8. Biernaux C, Loos M, Sels A, Huez G, Stryckmans P (1995) Detection of major bcr-abl gene expression at a very low level in blood cells of some healthy individuals. Blood 86:3118–3122
9. Bose S, Deininger M, Gora-Tybor J, Goldman JM, Melo JV (1998) The presence of typical and atypical BCR-ABL fusion genes in leukocytes of normal individuals: biologic significance and implications for the assessment of minimal residual disease. Blood 92:3362–3367
10. Clarkson BD, Strife A, Wisniewski D, Lambek C, Carpino N (1997) New understanding of the pathogenesis of CML: a prototype of early neoplasia. Leukemia 11:1404–1428
11. Eaves C, Cashman J, Eaves A (1998) Defective regulation of leukemic hematopoiesis in chronic myeloid leukemia. Leuk Res 22:1085–1096
12. Shepherd P, Suffolk R, Halsey J, Allan N (1995) Analysis of molecular breakpoint and m-RNA transcripts in a prospective randomized trial of interferon in chronic myeloid leukaemia: no correlation with clinical features, cytogenetic response, duration of chronic phase, or survival. Br J Haematol 89:546–554

13. Preston DL, Kusumi S, Tomonaga M, Izumi S, Ron E, Kuramoto A, Kamada N, Dohy H, Matsuo T, Matsui T (1994) Cancer incidence in atomic bomb survivors. Part III. Leukemia, lymphoma and multiple myeloma, 1950–1987. Radiat Res 137:68–97
14. Inskip PD, Kleinerman RA, Stovall M, Cookfair DL, Hadjimichael O, Moloney WC, Monson RR, Thompson WD, Wactawski-Wende J, Wagoner JK (1993) Leukemia, lymphoma, and multiple myeloma after pelvic radiotherapy for benign disease. Radiat Res 135:108–124
15. Boice JD Jr, Blettner M, Kleinerman RA, Stovall M, Moloney WC, Engholm G, Austin DF, Bosch A, Cookfair DL, Krementz ET (1987) Radiation dose and leukemia risk in patients treated for cancer of the cervix. J Natl Cancer Inst 79:1295–1311
16. Radivoyevitch T, Hoel DG (2000) Biologically-based risk estimation for radiation-induced chronic myeloid leukemia. Radiat Environ Biophys 39:153–159
17. Bauchinger M, Schmid E, Streng S, Dresp J (1983) Quantitative analysis of the chromosome damage at first division of human lymphocytes after ^{60}Co gamma-irradiation. Radiat Environ Biophys 22:225–229
18. Kellerer AM, Rossi HH (1978) A generalized formulation of dual radiation action. Radiat Res 75:471–488
19. Kozubek S, Lukasova E, Mareckova A, Skalnikova M, Kozubek M, Bartova E, Kroha V, Krahulcova E, Slotova J (1999) The topological organization of chromosomes 9 and 22 in cell nuclei has a determinative role in the induction of t(9, 22) translocations and in the pathogenesis of t(9, 22) leukemias. Chromosoma 108:426–435
20. Cucinotta FA, Nikjoo H, O'Neill P, Goodhead DT (2000) Kinetics of DSB rejoining and formation of simple chromosome exchange aberrations. Int J Radiat Biol 76:1463–1474
21. Lucas JN, Chen AM, Sachs RK (1996) Theoretical predictions on the equality of radiation-produced dicentrics and translocations detected by chromosome painting. Int J Radiat Biol 69:145–153
22. Knehr S, Zitzelsberger H, Braselmann H, Nahrstedt U, Bauchinger M (1996) Chromosome analysis by fluorescence in situ hybridization: further indications for a non-DNA-proportional involvement of single chromosomes in radiation-induced structural aberrations. Int J Radiat Biol 70:385–392
23. Lobrich M, Ikpeme S, Kiefer J (1994) Measurement of DNA double-strand breaks in mammalian cells by pulsed-field gel electrophoresis: a new approach using rarely cutting restriction enzymes. Radiat Res 138:186–192
24. Cedervall B, Wong R, Albright N, Dynlacht J, Lambin P, Dewey WC (1995) Methods for the quantification of DNA double-strand breaks determined from the distribution of DNA fragment sizes measured by pulsed-field gel electrophoresis. Radiat Res 143:8–16
25. Chen J, Nekolla E, Kellerer AM (1996) A comparative study of microdosimetric properties of x-rays, gamma- rays, and beta-rays. Radiat Environ Biophys 35:263–266
26. Lloyd DC, Edwards AA (1983) Chromosome aberrations in human lymphocytes: effect of radiation quality, dose, and dose rate. In: Ishihara T, Sasaki M (eds) Radiation-induced chromosome damage in man. Liss, New York, pp 23–49
27. Morton NE (1991) Parameters of the human genome. Proc Natl Acad Sci USA 88:7474–7476
28. Radivoyevitch T, Hoel DG (1999) Modeling the low-LET dose-response of BCR-ABL formation: predicting stem cell numbers from A-bomb data. Math Biosci 162:85–101
29. Neves H, Ramos C, da Silva MG, Parreira A, Parreira L (1999) The nuclear topography of ABL, BCR, PML, and RARα genes: evidence for gene proximity in specific phases of the cell cycle and stages of hematopoietic differentiation. Blood 93:1197–1207
30. Skalnikova M, Kozubek S, Lukasova E, Bartova E, Jirsova P, Cafourkova A, Koutna I, Kozubek M (2000) Spatial arrangement of genes, centromeres and chromosomes in human blood cell nuclei and its changes during the cell cycle, differentiation and after irradiation. Chromosome Res 8:487–499
31. Lukasova E, Kozubek S, Kozubek M, Kjeronska J, Ryznar L, Horakova J, Krahulcova E, Horneck G (1997) Localisation and distance between ABL and BCR genes in interphase nuclei of bone marrow cells of control donors and patients with chronic myeloid leukaemia. Hum Genet 100:525–535
32. Kozubek S, Lukasova E, Ryznar L, Kozubek M, Liskova A, Govorun RD, Krasavin EA, Horneck G (1997) Distribution of ABL and BCR genes in cell nuclei of normal and irradiated lymphocytes. Blood 89:4537–4545
33. Kellerer AM, Nekolla E (1997) Neutron versus gamma-ray risk estimates. Inferences from the cancer incidence and mortality data in Hiroshima. Radiat Environ Biophys 36:73–83
34. Harrison WJ (1962) The total cellularity of the bone marrow in man. J Clin Pathol 15:254–259
35. Berardi AC, Wang A, Levine JD, Lopez P, Scadden DT (1995) Functional isolation and characterization of human hematopoietic stem cells. Science 267:104–108
36. Radivoyevitch T, Ramsey MJ, Tucker JD (1999) Estimation of the target stem-cell population size in chronic myeloid leukemogenesis. Radiat Environ Biophys 38:201–206
37. Nikiforova MN, Stringer JR, Blough R, Medvedovic M, Fagin JA, Nikiforov YE (2000) Proximity of chromosomal loci that participate in radiation-induced rearrangements in human cells. Science 290:138–141
38. Ron E, Lubin JH, Shore RE, Mabuchi K, Modan B, Pottern LM, Schneider AB, Tucker MA, Boice JD Jr (1995) Thyroid cancer after exposure to external radiation: a pooled analysis of seven studies. Radiat Res 141:259–277